

# Organofluorosilanes as Model Compounds for $^{18}\text{F}$ -Labeled Silicon-Based PET Tracers and their Hydrolytic Stability: Experimental Data and Theoretical Calculations (PET = Positron Emission Tomography)

Aileen Höhne,<sup>[a]</sup> Lian Yu,<sup>[b]</sup> Linjing Mu,<sup>[a]</sup> Markus Reiher,<sup>\*,[b]</sup> Ulrike Voigtmann,<sup>[c]</sup> Ulrich Klar,<sup>[c]</sup> Keith Graham,<sup>[c]</sup> P. August Schubiger,<sup>[a]</sup> and Simon M. Ametamey<sup>\*,[a]</sup>

**Abstract:** Silicon chemistry has only recently been discovered by radiochemists as a straightforward tool for the introduction of  $^{18}\text{F}$  into biomolecules for positron emission tomography (PET) imaging.  $^{18}\text{F}$ -labeled PET tracers must be stable towards defluorination under physiological conditions, but it is known that the hydrolytic stability of the silicon–fluorine bond is determined by the nature of the substituents on silicon. In the presented study we performed an extensive investigation on

the hydrolytic stability of various synthesized organofluorosilane model compounds. By means of density functional theory (DFT) methods a theoretical model of organofluorosilane hydrolysis, which correlates with the experimentally determined hydrolytic

half-lives, is developed. The calculation of the difference of Si–F bond lengths between the optimized structures of the starting material **A** and the intermediate structure **C** allows the estimation of the hydrolytic stability of newly designed compounds. This model permits the facilitated development of improved building blocks for the synthesis of novel  $^{18}\text{F}$ -silyl-modified biomolecules for PET imaging.

**Keywords:** density functional calculations • hydrolysis • organofluorosilanes • positron emission tomography • synthesis design

## Introduction

Positron emission tomography (PET) is a non-invasive imaging technology permitting measurement of physiological, biochemical, and pharmacological functions at the molecular level. Radiolabeled biomolecules have many potential appli-

cations as probes for PET. Among the available PET nuclides,  $^{18}\text{F}$  has ideal characteristics regarding its half-life (109.7 min) and low  $\beta^+$  energy (0.64 MeV). Only recently, radiochemists have discovered silicon chemistry as a straightforward tool for the introduction of  $^{18}\text{F}$  into biomolecules.<sup>[1]</sup> Due to the high affinity of silicon for fluorine it is possible to introduce  $^{18}\text{F}$  into silicon-containing biomolecules under mild conditions through nucleophilic substitution with  $^{18}\text{F}^-$  by using an appropriate labeling precursor.

$^{18}\text{F}$ -labeled PET tracers must be stable towards defluorination under physiological conditions. If free fluoride is released in the blood by defluorination, it will accumulate in the bone. Consequently, defluorination of  $^{18}\text{F}$ -labeled radiopharmaceuticals in vivo becomes a hindrance for imaging, or leads to needless radiation exposure of patients.<sup>[2]</sup> It is known that the hydrolytic stability of the silicon–halogen bond is determined by the nature of the substituents on silicon. Based on these considerations, different organosilanes were proposed and used as labeling moieties.<sup>[1]</sup>

The kinetics and thermodynamics of the hydrolysis of organofunctional chloro- and especially alkoxy silanes have been studied extensively, due to the popularity of silyl ethers as protection groups in organic synthesis, and their

[a] A. Höhne, Dr. L. Mu, Prof. Dr. P. A. Schubiger, Prof. Dr. S. M. Ametamey  
Center for Radiopharmaceutical Science of ETH, PSI and USZ  
Department of Chemistry and Applied Biosciences  
ETH Zurich, 8093 Zurich (Switzerland)  
Fax: (+41) 44-633-1367  
E-mail: simon.ametamey@pharma.ethz.ch

[b] L. Yu, Prof. Dr. M. Reiher  
Laboratory of Physical Chemistry  
Department of Chemistry and Applied Biosciences  
ETH Zurich, 8093 Zurich (Switzerland)  
Fax: (+41) 44-633-1594  
E-mail: markus.reiher@phys.chem.ethz.ch

[c] Dr. U. Voigtmann, Dr. U. Klar, Dr. K. Graham  
Bayer Schering Pharma AG, Global Drug Discovery  
13342 Berlin (Germany)

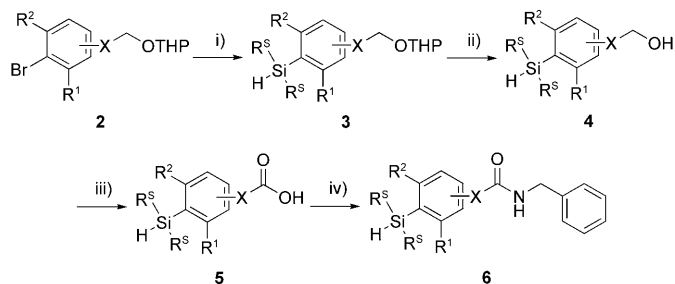
Supporting information for this article is available on the WWW under <http://dx.doi.org/10.1002/chem.200802437>.

large scale use, for instance for the production of silicones.<sup>[3]</sup> To our knowledge, so far only the hydrolysis of some simple organofluorosilanes has been investigated by theoretical methods.<sup>[4]</sup> Furthermore, Schirmacher et al. have confirmed the high efficiency of <sup>19</sup>F–<sup>18</sup>F isotopic exchange reactions of organofluorosilanes by DFT calculations on three model compounds (*t*Bu<sub>2</sub>PhSiF, *t*BuPh<sub>2</sub>SiF, Ph<sub>3</sub>SiF).<sup>[1g]</sup> The reaction is predicted to proceed, in accordance with the known mechanism of nucleophilic substitution at the silicon atom,<sup>[5]</sup> via a thermodynamically stable pentacoordinate silicate intermediate, dissociating immediately to form the radiolabeled product.

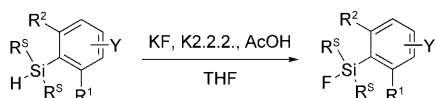
In the present study, we performed an extensive investigation on the hydrolytic stability of various synthesized organofluorosilane model compounds (Table 1, **1a–o**). We asked the question whether it would be possible to develop a theoretical model of hydrolysis that correlates with our experimental data. By answering this question we hoped to better understand the detailed factors influencing the stability of the Si–F bond and so be able to predict the stability of newly designed compounds. Based on the theoretical calculations and the experimental hydrolytic half-lives, two building blocks were selected for coupling to target bombesin peptides.

## Results and Discussion

**Synthesis of silicon model compounds:** The syntheses of the organofluorosilanes are outlined in Schemes 1 and 2. The arylbromides **2** were metalated at 0 °C by using dibutylisopropylmagnesate, which was formed in situ from isopropylmagnesium chloride and *n*-butyllithium.<sup>[6]</sup> The resulting arylmag-



Scheme 1. Synthesis of precursors for fluorination; X = *p*-O(CH<sub>2</sub>)<sub>2</sub>, (*p*-CH<sub>2</sub>)<sub>0</sub>, *p*-CH<sub>2</sub>, *m*-CH<sub>2</sub>, or *p*-(CH<sub>2</sub>)<sub>2</sub>; R<sup>1</sup>, R<sup>2</sup> = H or Me; R<sup>S</sup> = *i*Pr, *t*Bu, or Ph. Reagents and conditions: i) method 1: (*i*Pr)<sub>2</sub>Bu<sub>2</sub>MgLi, THF, 0 °C, 2 h, then (R<sup>S</sup>)<sub>2</sub>SiHCl, RT, 2 h (93–99%); method 2: *n*BuLi, THF, –78 °C, 1 h, then *i*Pr<sub>2</sub>SiHCl, RT, 40 h (98%); ii) method 1: *p*-TsOH, EtOH, RT, 4 h (70–93% or crude); method 2: PPTS, EtOH, 55 °C, 3 h (72%); iii) Jones reagent, acetone, 0 °C, 15 min (61–64% over two steps or 72% from pure alcohol); iv) EDC-HCl, benzylamine, CH<sub>2</sub>Cl<sub>2</sub>, RT, 19–24 h (65–80%).



Scheme 2. Synthesis of fluorosilanes **1**.

Table 1. Organofluorosilanes under investigation and their hydrolytic half-lives (*t*<sub>1/2</sub>).

Compound	Structure	<i>t</i> <sub>1/2</sub>
<b>1a</b>		≤ 5 min
<b>1b</b>		6 min
<b>1c</b>		8 h
<b>1d</b>		12 h
<b>1e</b>		15 h
<b>1f</b>		21 h
<b>1g</b>		29 h
<b>1h</b>		37 h
<b>1i</b>		37 h
<b>1j</b>		43 h
<b>1k</b>		61 h
<b>1l</b>		79 h
<b>1m</b>		302 h

Table 1. (Continued)

Compound	Structure	$t_{1/2}$
<b>1n</b>		> 300 h
<b>1o</b>		> 300 h <sup>[a]</sup>

[a] No hydrolysis observed within 170 h.

nesium intermediates were coupled with diisopropyl-, diisobutyl-, or diphenylchlorosilane to give the corresponding arylsilanes **3** in 93–99% yield. Based on good experience with the use of the less sterically demanding reagent *n*-butyllithium for the synthesis of hindered silanes,<sup>[1h]</sup> we employed these conditions for the synthesis of the *ortho*-dimethylaryl substituted silane (**3** with  $R^S = iPr$ ;  $X = O(CH_2)_2$ ;  $R^1, R^2 = Me$ ) and obtained the product in very high yield. In the next step, THP-protected arylsilanes (THP=tetrahydropyran) were converted into the free alcohols **4** using *p*-toluenesulfonic acid. These conditions gave, after the deprotection of the *ortho*-dimethylaryl substituted silane, the desilylation product as the main product. Using the less acidic deprotection agent pyridinium *p*-toluenesulfonate (PPTS),<sup>[7]</sup> the desired alcohol was obtained in 72% yield. Alcohols **4a–c** ( $R^S = iPr$ ;  $X = O(CH_2)_2$ ;  $R^1, R^2 = H$  or  $Me$ ) were converted into the corresponding carboxylic acids **5a–c** with Jones reagent. The obtained carboxylic acid building blocks were coupled with benzyl amine in 65–80% yield. Finally, the fluorination of a series of hydrosilanes with different substitution patterns was carried out under acidic conditions to obtain the organofluorosilanes of interest.

**Hydrolytic stability studies of synthesized organofluorosilanes:** <sup>18</sup>F-labeled PET tracers should be stable towards defluorination under physiological conditions. Therefore, model compounds **1a–o** were tested for their hydrolytic stability. For a straightforward data analysis pseudo-first-order kinetics were assumed (Table 1). The hydrolytic stabilities of the dimethyl- and diphenyl-substituted fluorosilanes proved to be very low. After just five minutes in aqueous solution, fluorosilane **1a** was no longer detectable by HPLC. For **1b** a hydrolytic half-life of six minutes was determined. The diisobutyl fluorosilane **1f** ( $t_{1/2} = 21$  h) was significantly less stable than its diisopropyl analogue **1i** (79 h). The degree of hydrolytic stability of diisopropyl fluorosilanes depends on their further substitution pattern (Figure 1). There is a decrease in hydrolytic stability in the order THP ether (**1l**,  $t_{1/2} = 79$  h) > alcohol (**1j**, 43 h) > carboxylic acid (**1h**, 37 h) > amide (**1c**, 8 h). As our method of biomolecule modification comprises the introduction of silicon-containing building blocks through coupling of the appropriate carboxylic acid derivatives to a free amine,<sup>[1h]</sup> only an amide can be consid-

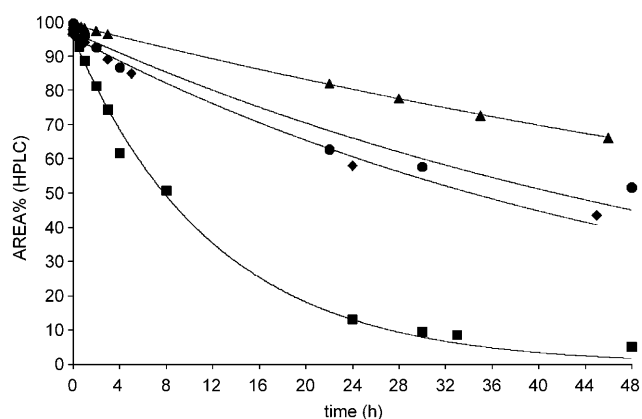


Figure 1. Hydrolytic stability curves for fluorosilanes **1c** (■), **1h** (◆), **1j** (●), and **1l** (▲).

ered as a reliable model for <sup>18</sup>F-labeled silyl-modified biomolecules.

The dependency of stability on remote functionalities is remarkable. To provide further evidence, alcohols differing in alkyl chain length and position were studied (Figure 2).

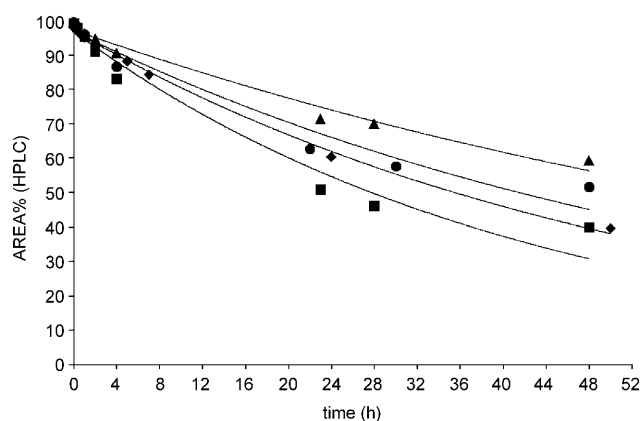


Figure 2. Hydrolytic stability curves for fluorosilanes **1g** (■), **1i** (◆), **1j** (●), and **1k** (▲).

The following tendency of stability was observed: *p*-(CH<sub>2</sub>)<sub>3</sub> (**1k**,  $t_{1/2} = 61$  h) > *p*-(CH<sub>2</sub>)<sub>2</sub> (**1j**, 43 h) > *p*-CH<sub>2</sub> (**1i**, 37 h) > *m*-(CH<sub>2</sub>)<sub>2</sub> (**1g**, 29 h), although the differences are not so pronounced as for the different functionalities. The diisopropyl silyl amides **1c**, **1d**, and **1e** have very similar hydrolytic half-lives (8, 12, and 15 h, respectively) despite containing different linkers.

As the improvement in stability through increase of steric hindrance around the silicon atom was found to be especially significant (see di-*tert*-butyl derivative **1o**),<sup>[1h]</sup> the *ortho*-monomethyl- and dimethyl-substituted analogues of fluorosilane **1e** were tested (Figure 3). We observed a dramatic increase in stability for the monomethyl-substituted analogue **1m** ( $t_{1/2} = 302$  h), which was further enhanced by another *ortho*-methyl group in **1n**. No hydrolyzed product was observed during the study period.

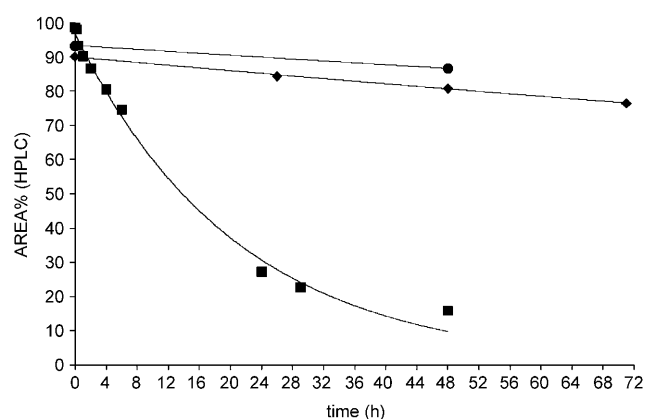


Figure 3. Hydrolytic stability curves for fluorosilanes **1e** (■), **1m** (◆), and **1n** (●).

In summary, the very bulky derivatives **1n** and **1o** are outstanding in their stability. A drawback regarding the pharmacokinetic behavior of biomolecules containing these building blocks might be their relatively high lipophilicity ( $c\log P=6.10$  for **1n** and  $c\log P=5.56$  for **1o**), which in some cases can be compensated for by other polar functionalities present in the biomolecule. In addition, the silicon-aryl bond in **1n** is not very stable and therefore prone to cleavage, as shown by the desilylation during deprotection of the *ortho*-dimethylaryl substituted silane (**3** with  $R^S=iPr$ ;  $X=O(CH_2)_2$ ;  $R^1, R^2=Me$ ) with *p*-toluenesulfonic acid. We hypothesized that a theoretical model of hydrolytic stability that correlated with our experimental data might allow us to design new compounds with similar stability, but lower lipophilicity than **1n** and **1o**.

**Theoretical calculations:** To find a suitable DFT functional to describe accurately the fluorinated organosilicon compounds, we selected a 2-(phenylazo)phenyl allyldifluorosilane as a reference compound, as it is similar to the organosilicon compounds under consideration and has already been characterized by X-ray crystallographic analysis (Figure 4).<sup>[8]</sup>

As shown by the data in Table 2, the BP86 and B3LYP functionals were apparently not good enough to describe the molecular structure. In contrast, the functionals TPSS and TPSSH yielded much better results that are very close to the experimental measurements. To reproduce accurately the Si–F bonds, we used the larger basis set TZVPP for the Si atoms. Owing to the RI technique, the pure functional TPSS allows quicker calculations compared to the hybrid functional TPSSH. Therefore we selected the TPSS/RI/TZVP(P) combination of density functional and basis set for our DFT calculations.

Fluorosilanes **1a**, **1c–e**, **1i–k** and **1m–o** were selected for the DFT calculations. Figure 5 shows the optimized structures for the selected compounds obtained with TPSS/RI/TZVP(P). The environment of the silicon atoms for all compounds is similar and the ligand exchange energies of all compounds are not large (Table 3), which indicates that ex-

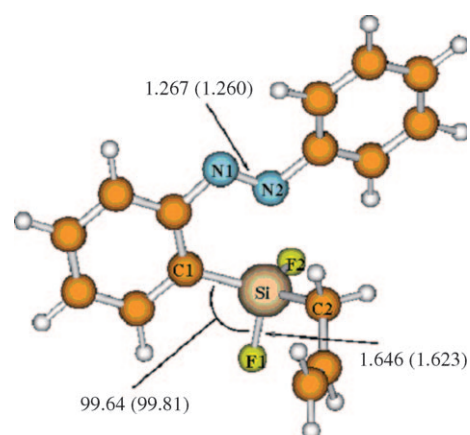


Figure 4. TPSS/RI/TZVP(P) optimized structure of 2-(phenylazo)phenyl allyldifluorosilane. Bond lengths are given in Ångströms and bond angles in degrees. Experimental data are given in parentheses. Hydrogen atoms: white; carbon atoms: brown; nitrogen atoms: blue; fluorine atoms: yellow; silicon atoms: light brown.

Table 2. Selected bond lengths (Å) for optimized structures of 2-(phenylazo)phenyl allyldifluorosilane.<sup>[a]</sup>

	Si–N2	Si–F1	Si–F2	Si–C1	Si–C2
BP86/RI/TZVP	2.501	1.664	1.650	1.892	1.906
B3LYP/TZVP	2.589	1.645	1.633	1.885	1.894
TPSS/RI/TZVP	2.390	1.662	1.647	1.885	1.905
TPSSH/TZVP	2.401	1.652	1.638	1.881	1.897
TPSS/RI/TZVP(P)	2.394	1.646	1.631	1.881	1.900
experiment	2.389	1.623	1.596	1.858	1.864

[a] TZVP(P) refers to the TZVPP basis set only for the Si atom and the TZVP basis set for all of the other atom.

change of  $F^-$  versus  $HO^-$  is thermodynamically feasible, with the OH derivatives being more stable than the F derivatives. Neither the bond lengths and angles nor the partial charges and ligand exchange energies show a correlation with the experimentally determined hydrolytic half-lives of the corresponding substances.

Scheme 3 shows a possible  $S_N2$  mechanism for the hydrolysis of the Si–F bond, which, according to our calculations, occurs most probably under inversion. The proposed pathway is in accordance with the known mechanism of nucleophilic substitution at the silicon atom, which is believed to proceed via a pentacoordinate intermediate.<sup>[5]</sup> The Si–F bond lengths of the optimized intermediate structures **C** (Figure 6) are an essential factor for this hydrolysis reaction. As shown by the data in Table 4, the distance between the O atom in  $HO^-$  and the Si atom is shorter than the bond length of Si–F. When the Si–F bond length is short, the F atom binds strongly to the Si atom, so that hydrolysis is difficult to accomplish. This mechanism should not be taken too literally, since it was obtained by consideration of micro-solvated model structures only. However, these details are not important for the quantitative concept designed for the stability prediction of the Si–F bond against hydrolysis, as we shall see. In fact, we did not optimize the transition state structure, since the stable intermediate **C** already serves our

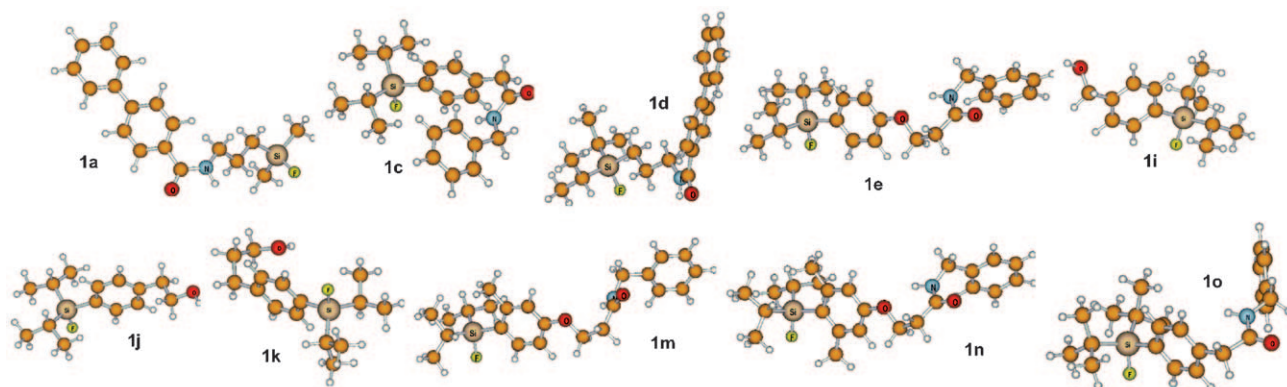
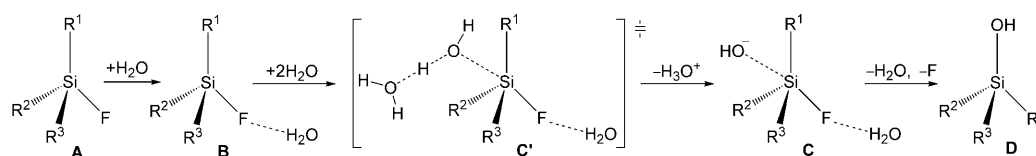


Figure 5. Optimized structures obtained with TPSS/RI/TZVP(P) for compounds **1a–o**. Hydrogen atoms: white; carbon atoms: brown; nitrogen atoms: blue; oxygen atoms: red; fluorine atoms: yellow; silicon atoms: light brown.

Table 3. Selected bond lengths, angles, partial charges, and ligand exchange energies ( $R-F + HO^- \rightarrow R-OH + F^-$ ) for compounds **1a–o** obtained with TPSS/RI/TZVP(P).<sup>[a]</sup>

	Bond lengths [Å]			Bond angles [°]		Partial charges			Ligand exchange energy [kJ mol <sup>-1</sup> ]	<i>t</i> <sub>1/2</sub> [h]	
	Si–F	Si–R <sup>L</sup>	Si–R <sup>S</sup>	F–Si–R <sup>L</sup>	F–Si–R <sup>S</sup>	Si	F	C(R <sup>L</sup> )			C(R <sup>S</sup> )
<b>1a</b>	1.638	1.890	1.878	105.89	106.98	1.87	–0.63	–0.86	–1.10	–43.1	0
<b>1c</b>	1.640	1.888	1.902	105.70	106.77	1.92	–0.64	–0.50	–0.66	–43.3	8
<b>1d</b>	1.644	1.894	1.900	105.35	105.53	1.92	–0.64	–0.88	–0.67	–41.3	12
<b>1e</b>	1.641	1.883	1.899	105.37	105.66	1.92	–0.64	–0.53	–0.66	–43.5	15
<b>1i</b>	1.641	1.886	1.900	104.91	106.34	1.92	–0.64	–0.50	–0.66	–40.5	37
<b>1j</b>	1.641	1.885	1.903	105.73	106.62	1.92	–0.64	–0.51	–0.66	–42.3	43
<b>1k</b>	1.642	1.882	1.901	105.49	106.08	1.92	–0.64	–0.51	–0.66	–41.6	61
<b>1m</b>	1.644	1.890	1.905	103.36	104.78	1.93	–0.65	–0.53	–0.67	–49.6	302
<b>1n</b>	1.648	1.906	1.914	108.47	105.72	1.96	–0.65	–0.53	–0.68	–35.7	∞
<b>1o</b>	1.644	1.892	1.921	103.93	104.44	2.02	–0.66	–0.53	–0.49	–42.0	∞

[a] R<sup>L</sup> = larger substituent group on the silicon atom. R<sup>S</sup> = two smaller substituent groups on the silicon atom. C(R<sup>L</sup>) means the Si-connected C atom in the larger substituent group. C(R<sup>S</sup>) refers to the C atoms in the two smaller substituent groups.



Scheme 3. S<sub>N</sub>2 mechanism (with H<sub>2</sub>O as a spectator) of the hydrolysis reaction for the organofluorosilanes.

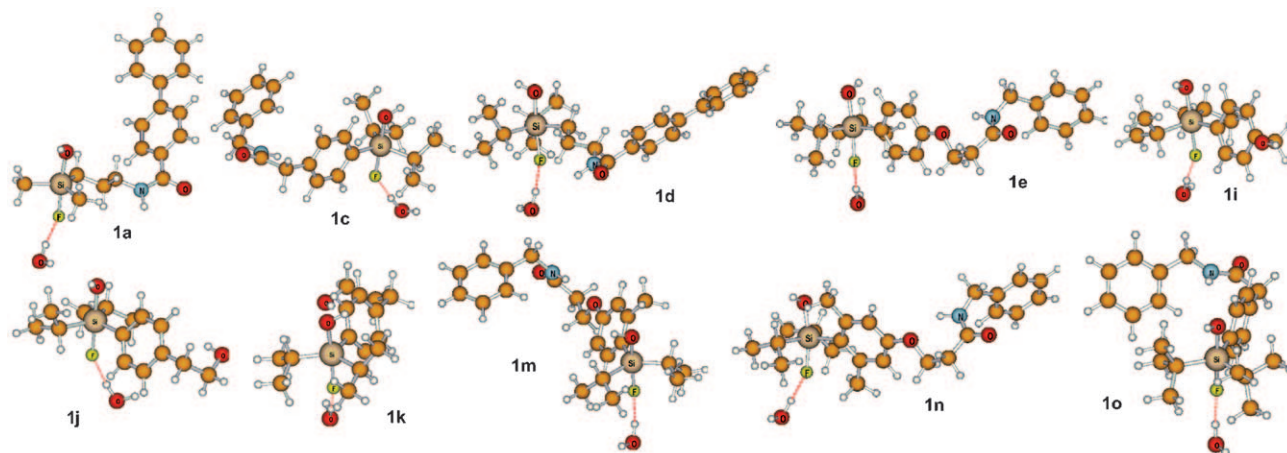


Figure 6. Optimized intermediate structures **C** obtained with TPSS/RI/TZVP(P) for compounds **1a–o**. Hydrogen atoms: white; carbon atoms: brown; nitrogen atoms: blue; oxygen atoms: red; fluorine atoms: yellow; silicon atoms: light brown.

Table 4. Selected bond lengths and angles of the optimized intermediate structure **C**, and difference of Si–F bond lengths between the optimized structures **A** and **C** ( $\Delta_{(\text{Si-F})}$ ) obtained with TPSS/RI/TZVP(P) for compounds **1a–o**.

	Bond lengths [Å]			Bond angles [°]		$\Delta_{(\text{Si-F})}$ [Å]	$t_{1/2}$ [h]
	Si–F	Si–OH	Si–R <sup>L</sup>	F–Si–OH	F–Si–R <sup>L</sup>		
<b>1a</b>	1.872	1.798	1.934	172.82	84.75	0.234	0
<b>1c</b>	1.861	1.791	1.950	176.30	87.63	0.221	8
<b>1d</b>	1.865	1.797	1.935	173.50	84.62	0.221	12
<b>1e</b>	1.864	1.811	1.947	175.29	89.38	0.223	15
<b>1i</b>	1.859	1.792	1.942	173.37	89.63	0.218	37
<b>1j</b>	1.855	1.794	1.945	174.66	89.30	0.214	43
<b>1k</b>	1.853	1.795	1.946	174.56	89.40	0.211	61
<b>1m</b>	1.831	1.805	1.953	170.22	90.44	0.187	302
<b>1n</b>	1.817	1.794	1.988	165.52	94.47	0.169	>300
<b>1o</b>	1.827	1.791	1.961	175.05	86.96	0.183	>300

purposes (because all reaction steps that produce **C** from **A** can be considered reversible). We should emphasize, however, that the microsolvated structures chosen for Scheme 3 have not been selected randomly. Instead, we performed structure optimization of different microsolvated structures. One might think, for example, that up to three water molecules could be bound to the fluorine atom in the Si–F bond, but the microsolvated structures show that this is not the case. If we start a structure optimization from a triply hydrated fluorine atom this leads to the dissociation of two of the three water molecules. While one is then hydrogen-bonded to the water molecule that still coordinates to the fluorine atom, the third one binds easily to any other polar atom in the molecule. Hence, it is sufficient to consider only a single water molecule in our model, which we would like to be as simple, but also as efficient, as possible.

If less than about 5% defluorination after 6 h is accepted as the criterion for a stable compound allowing the realization of a PET study, a hydrolytic half-life of approximately 81 h arises as the minimum requirement for stability. Accordingly, the following trend (Figure 7) can be derived from the differences of Si–F bond lengths between the optimized structures **A** and **C** (Table 4): compounds with  $\Delta_{(\text{Si-F})}$

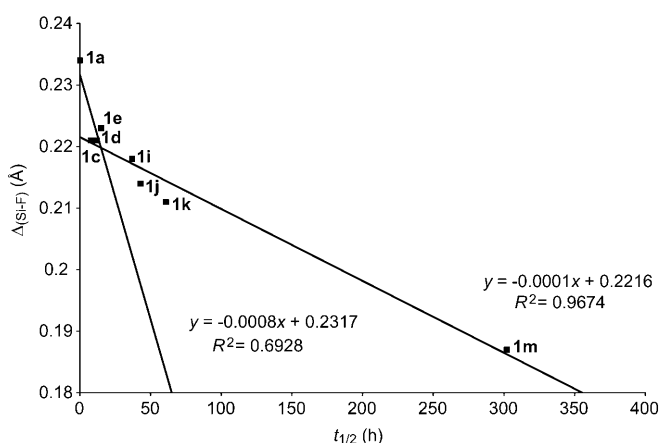


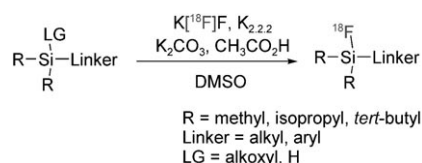
Figure 7. Hydrolytic half-lives ( $t_{1/2}$ ) of selected fluorosilanes versus differences of Si–F bond lengths ( $\Delta_{(\text{Si-F})}$ ) between the optimized structures of starting material **A** and intermediate **C**. Trendline obtained by linear regression analysis considering **1c–e**, **1i–k**, and **1m**.

$\Delta_{(\text{Si-F})} \geq 0.211 \text{ \AA}$  are relatively unstable ( $t_{1/2} < 81 \text{ h}$ ); the ones with  $\Delta_{(\text{Si-F})} \leq 0.187 \text{ \AA}$  are stable according to our criterion ( $t_{1/2} \geq 81 \text{ h}$ ). Additionally, the influence of small changes in the larger substituent group on the silicon atom ( $\text{R}^L$ ) is reflected by the model: the difference of Si–F bond lengths between the optimized structures **A** and **C** for **1c** ( $0.221 \text{ \AA}$ ,  $t_{1/2} = 8 \text{ h}$ ) is larger than for **1j** ( $0.214 \text{ \AA}$ ,  $t_{1/2} = 43 \text{ h}$ ), and for **1i** ( $0.218 \text{ \AA}$ ,  $t_{1/2} = 37 \text{ h}$ ) larger than for **1k** ( $0.211 \text{ \AA}$ ,  $t_{1/2} = 61 \text{ h}$ ).

The linear correlation of the half-lives and the change in the Si–F bond length from **A** to **C** (Figure 7) can be rationalized as follows. First of all, the Si–F bond length in structure **C** is activated, because of the hydroxyl group coordinated to the silicon atom and because of the water molecule that enhances the leaving group character of the fluorine ion. Hence, the longer the bond length the more activated the fluorine atom should be and the faster hydrolysis should occur. However, since all Si–F bonds in the different molecules **A** under consideration feature different equilibrium bond lengths, the activation of the Si–F bond in **C** can only be measured against the equilibrium bond length in the corresponding structure **A**. Consequently, the bond length difference should be an appropriate measure, and the linear behavior highlighted by Figure 7 confirms this assumption.

If we consider model compounds **1a**, **1c**, **1d**, and **1e** with half-lives less than 15 h, a poor linear correlation ( $R^2 = 0.69$ , Figure 7) of  $\Delta_{(\text{Si-F})}$  and  $t_{1/2}$  is observed. Because **1a** is distant from the linear relationship between  $\Delta_{(\text{Si-F})}$  and  $t_{1/2}$  (Figure 7), it is reasonable to exclude **1a** from the linear regression analysis. Indeed, exclusion of **1a** results in a better correlation of the data ( $R^2 = 0.97$ ). Compound **1a** is a special case, because it hydrolyzes immediately in aqueous solution and is the least stable compound among all the fluorosilanes examined. We speculate this might be due to the much better accessibility of the silicon atom in **1a** compared to the other more bulky fluorosilanes, and therefore faster kinetics of the exchange of F for OH. The hydrolytic half-life of **1n** goes to infinity and lies outside the scale of Figure 7. This is also the case for **1o**, which showed no hydrolysis after 170 h. However, if  $t_{1/2}$  of **1n** and **1o** are calculated from their  $\Delta_{(\text{Si-F})}$  values, hydrolytic half-lives of 449 h and 330 h, respectively, are extrapolated. All in all, the linearity of the model is, to a certain degree, disturbed at the two extremes of the scale. The hydrolytic half-lives are presumably influenced by different kinetic and/or equilibrium effects depending on the bulkiness of the organic substituents on Si.

**<sup>18</sup>F radiolabeling:** The <sup>18</sup>F labeling of the silicon model compounds is depicted in Scheme 4. The influence of temperature and that of acetic acid as an additive were also investi-



Scheme 4. <sup>18</sup>F radiolabeling of synthesized silicon model compounds.



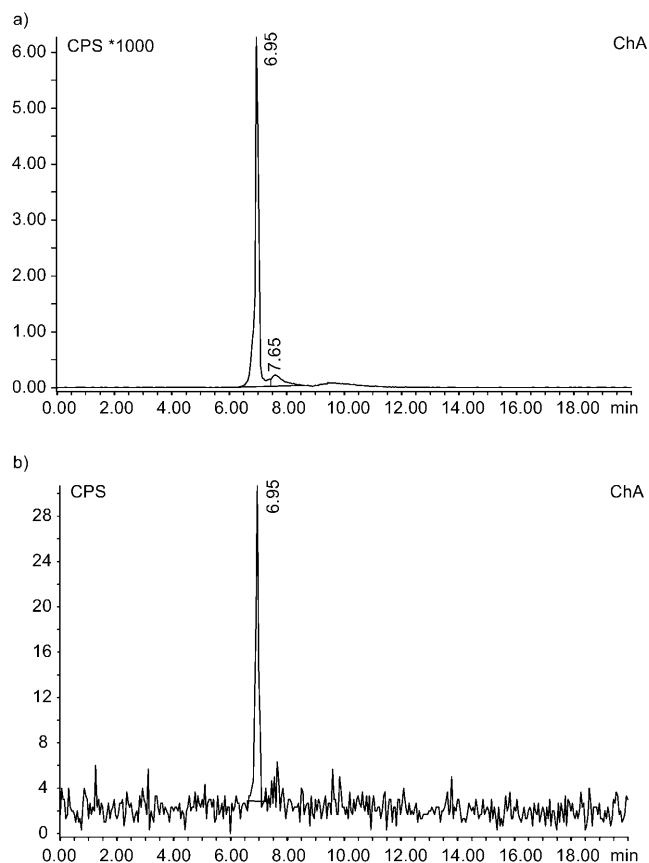


Figure 8. Radio-HPLC chromatograms of 2-(4-(di-tert-butyl-<sup>18</sup>F)fluorosilyl)phenyl)acetyl-Arg-Ava-Gln-Trp-Ala-Val-NMeGly-His-Sta-Leu-NH<sub>2</sub> (<sup>18</sup>F-**1q**) after 2 h: a) in phosphate buffer; b) in mouse plasma.

### Computational Methods

The all-electron Kohn–Sham DFT calculations were performed with the quantum-chemical program package Turbomole.<sup>[11]</sup> In the DFT calculations the pure functionals BP86<sup>[12]</sup> and TPSS<sup>[13]</sup> in combination with the resolution-of-the-identity (“RI”) density fitting technique, and also the hybrid functionals B3LYP<sup>[14]</sup> and TPSSH<sup>[15]</sup> were applied. The TZVP and TZVPP basis sets by Schäfer et al.<sup>[16]</sup> were employed for the DFT calculations. For the calculation of partial charges, natural population analysis as implemented in Gaussian 03 was used.<sup>[17]</sup> The molecular structures were visualized with the program Molden.<sup>[18]</sup> All geometry optimizations were performed in C<sub>1</sub> symmetry.

### Acknowledgement

We gratefully acknowledge Marion Kuzora for technical assistance.

[1] a) J. C. Walsh, K. M. Akhooon, N. Stayamurthy, J. R. Barrio, M. E. Phelps, S. S. Gambhir, T. Toyokuni, *J. Labelled Compd. Radiopharm.* **1999**, *42*, S1-S3; b) R. Ting, M. J. Adam, T. J. Ruth, D. M. Perrin, *J. Am. Chem. Soc.* **2005**, *127*, 13094–13095; c) U. Choudhry, K. E. Martin, S. Biagini, P. J. Blower, *Nucl. Med. Commun.* **2006**, *27*, 293; d) U. Choudhry, K. Martin, D. Mainard, S. C. G. Biagini, P. J. Blower, *Eur. J. Nucl. Med. Mol. Imaging* **2006**, *33*, S306; e) U. Choudhry, R. Paul, S. C. G. Biagini, P. J. Blower, *Eur. J. Nucl. Med. Mol. Imaging* **2007**, *34*, S332; f) R. Schirmmacher, G. Bradtmöller, E.

Schirmmacher, O. Thews, J. Tillmanns, T. Siessmeier, H. G. Bucholz, P. Bartenstein, B. Wängler, C. M. Niemeyer, K. Jurkschat, *Angew. Chem.* **2006**, *118*, 6193–6197; *Angew. Chem. Int. Ed.* **2006**, *45*, 6047–6050; g) E. Schirmmacher, B. Wängler, M. Cypryk, G. Bradtmöller, M. Schäfer, M. Eisenhut, K. Jurkschat, R. Schirmmacher, *Bioconjugate Chem.* **2007**, *18*, 2085–2089; h) L. Mu, A. Höhne, P. A. Schubiger, S. M. Ametamey, K. Graham, J. E. Cyr, L. Dinkelborg, T. Stellfeld, A. Srinivasan, U. Voigtmann, U. Klar, *Angew. Chem.* **2008**, *120*, 5000–5003; *Angew. Chem. Int. Ed.* **2008**, *47*, 4922–4925.

[2] Y. Magata, L. Lang, D. O. Kiesewetter, E. M. Jagoda, M. A. Channing, W. C. Eckelman, *Nucl. Med. Biol.* **2000**, *27*, 163–168.

[3] a) R. J. P. Corriu, G. Dabosi, M. Martineau, *J. Organomet. Chem.* **1978**, *150*, 27–38; b) T. Kudo, M. S. Gordon, *J. Phys. Chem. A* **2002**, *106*, 11347–11353; c) F. D. Osterholtz, E. R. Pohl, *J. Adhes. Sci. Technol.* **1992**, *6*, 127–149; d) S. A. French, A. A. Sokol, C. R. A. Catlow, A. Kornherr, G. E. Nauer, G. Zifferer, *J. Chem. Phys.* **2006**, *124-125*, 24311–24317; e) P. J. Kocienski, *Protecting Groups*, 3rd ed., Thieme, Stuttgart, **2005**, Chapter 4.2.

[4] M. Cypryk, *J. Phys. Chem. A* **2005**, *109*, 12020–12026.

[5] a) A. R. Bassindale, P. G. Taylor in *The Chemistry of Organic Silicon Compounds* (Eds. S. Patai, Z. Rappoport), Wiley, New York, **1989**, Chapter 13; b) A. R. Bassindale, S. J. Glynn, P. G. Taylor in *The Chemistry of Organic Silicon Compounds, Vol. 2* (Eds.: S. Patai, Z. Rappoport), Wiley, New York, **1998**, Chapter 9.

[6] A. Inoue, K. Kitagawa, H. Shinokubo, K. Oshima, *J. Org. Chem.* **2001**, *66*, 4333–4339.

[7] M. Miyashita, A. Yoshikoshi, P. A. Grieco, *J. Org. Chem.* **1977**, *42*, 3772–3774.

[8] N. Kano, M. Yamamura, T. Kawashima, *J. Am. Chem. Soc.* **2004**, *126*, 6250–6251.

[9] W. C. Chan, P. D. White, *Fmoc Solid Phase Peptide Synthesis—A Practical Approach*, Oxford University Press, Oxford, **2003**.

[10] A. Höhne, L. Mu, P. A. Schubiger, S. M. Ametamey, K. Graham, T. Stellfeld, S. Borkowski, D. Berndorff, U. Klar, U. Voigtmann, J. E. Cyr, M. Friebe, L. Dinkelborg, A. Srinivasan, *Bioconjugate Chem.* **2008**, *19*, 1871–1879.

[11] R. Ahlrichs, M. Bär, M. Häser, H. Horn, C. Kölmel, *Chem. Phys. Lett.* **1989**, *162*, 165–169.

[12] a) A. D. Becke, *Phys. Rev. A* **1988**, *38*, 3098–3100; b) J. P. Perdew, *Phys. Rev. B* **1986**, *33*, 8822–8824.

[13] J. Tao, J. P. Perdew, V. N. Staroverov, G. E. Scuseria, *Phys. Rev. Lett.* **2003**, *91*, 146401.

[14] a) A. D. Becke, *J. Chem. Phys.* **1993**, *98*, 5648–5652; b) C. Lee, W. Yang, R. G. Parr, *Phys. Rev. B* **1988**, *37*, 785–789.

[15] V. N. Staroverov, G. E. Scuseria, J. Tao, J. P. Perdew, *J. Chem. Phys.* **2003**, *119*, 12129–12137.

[16] A. Schäfer, C. Huber, R. Ahlrichs, *J. Chem. Phys.* **1994**, *100*, 5829.

[17] Gaussian 03, Revision D.01, M. J. Frisch, G. W. Trucks, H. B. Schlegel, G. E. Scuseria, M. A. Robb, J. R. Cheeseman, J. A. Montgomery, Jr., T. Vreven, K. N. Kudin, J. C. Burant, J. M. Millam, S. S. Iyengar, J. Tomasi, V. Barone, B. Mennucci, M. Cossi, G. Scalmani, N. Rega, G. A. Petersson, H. Nakatsuji, M. Hada, M. Ehara, K. Toyota, R. Fukuda, J. Hasegawa, M. Ishida, T. Nakajima, Y. Honda, O. Kitao, H. Nakai, M. Klene, X. Li, J. E. Knox, H. P. Hratchian, J. B. Cross, V. Bakken, C. Adamo, J. Jaramillo, R. Gomperts, R. E. Stratmann, O. Yazyev, A. J. Austin, R. Cammi, C. Pomelli, J. W. Ochterski, P. Y. Ayala, K. Morokuma, G. A. Voth, P. Salvador, J. J. Dannenberg, V. G. Zakrzewski, S. Dapprich, A. D. Daniels, M. C. Strain, O. Farkas, D. K. Malick, A. D. Rabuck, K. Raghavachari, J. B. Foresman, J. V. Ortiz, Q. Cui, A. G. Baboul, S. Clifford, J. Ciołowski, B. B. Stefanov, G. Liu, A. Liashenko, P. Piskorz, I. Komaromi, R. L. Martin, D. J. Fox, T. Keith, M. A. Al-Laham, C. Y. Peng, A. Nanayakkara, M. Challacombe, P. M. W. Gill, B. Johnson, W. Chen, M. W. Wong, C. Gonzalez, J. A. Pople, Gaussian, Inc., Pittsburgh PA, **2004**.

[18] G. Schaftenaar, J. H. Noordik, *J. Comput.-Aided Mol. Des.* **2000**, *14*, 123.

Received: November 21, 2008  
Published online: March 6, 2009